

Article

Superoxide Radical Formed on the TiO₂ Surface Produced from Ti(OiPr)₄ Exposed to H₂O₂/KOH

Rimma I. Samoilova¹ and Sergei A. Dikanov^{2,*} 

¹ Voevodsky Institute of Chemical Kinetics and Combustion, Russian Academy of Sciences, Novosibirsk 630090, Russia; samoilov@kinetics.nsc.ru

² Department of Veterinary Clinical Medicine, University of Illinois at Urbana-Champaign, Urbana, IL 61801, USA

* Correspondence: dikanov@illinois.edu

Abstract: In this study, the superoxide radical O₂^{•−} formed by treating Ti(OR)₄ (R = iPr, nBu) with H₂O₂ in the presence of KOH was detected in the EPR spectra. The g-tensor of this radical differs from the typical values reported for a superoxide on various TiO₂ surfaces. On the other hand, similar g-tensor components g_{||}(zz = 2.10 ± 0.01, g_⊥ = 2.005 ± 0.003 assigned to the O₂^{•−} were previously observed for radicals in aqueous solutions in the presence of K₂O, alkaline solutions of DMSO, and water/DMSO mixtures. A common factor in all these systems is the presence of alkali ions. However, there was no structural support for the possible interaction of alkali ions with a superoxide in these systems. The use of multifrequency pulsed EPR techniques in this work revealed the stabilization of the O₂^{•−} near the K⁺ ion and its involvement in a strong hydrogen bond with the surface. These findings are consistent with the features previously reported for superoxides on a Na pre-covered MgO surface. Interactions with a closely located ²³Na and a strongly coupled ¹H proton were also seen in the HYSCORE spectra but assigned to two different superoxides with various g_{zz} values presented in the sample.

Keywords: TiO₂; hydrogen peroxide H₂O₂; KOH; superoxide radical; pulsed EPR; hyperfine coupling



Citation: Samoilova, R.I.; Dikanov, S.A. Superoxide Radical Formed on the TiO₂ Surface Produced from Ti(OiPr)₄ Exposed to H₂O₂/KOH. *Inorganics* **2023**, *11*, 274. <https://doi.org/10.3390/inorganics11070274>

Academic Editors: Hicham Idriss, Eleonora Aneggi, Richard Walton, Roberto Nisticò, Torben R. Jensen and Luciano Carlos

Received: 8 May 2023
Revised: 11 June 2023
Accepted: 24 June 2023
Published: 27 June 2023



Copyright: © 2023 by the authors. Licensee MDPI, Basel, Switzerland. This article is an open access article distributed under the terms and conditions of the Creative Commons Attribution (CC BY) license (<https://creativecommons.org/licenses/by/4.0/>).

1. Introduction

Superoxide anion (O₂^{•−}) is a radical formed after the one-electron reduction of dioxygen O₂, in different chemical processes [1]. In reactions with organic compounds, it can behave as a base, a nucleophile, and an oxidizing or reducing agent [2,3]. O₂^{•−} is paramagnetic, which has allowed for broad applications of multifrequency, continuous wave (CW) EPR spectroscopy for its studies [4–8].

The treatment of an oxide with a solution of hydrogen peroxide (H₂O₂), followed by drying the obtained solid under a vacuum has been also employed for generations of the superoxide radicals [9]. A product with matrix-bound O₂^{•−}, produced by treating Ti(OR)₄ (R = iPr, nBu) with H₂O₂, was described and used as a selective heterogeneous catalyst for the oxidation of organic compounds [10]. It is effective at room temperatures and with various solvents including water.

Detailed studies of the catalyst using various experimental methods have shown that O₂^{•−} is responsible for the reaction, and its exceptional stability results from a stabilization near Ti⁴⁺ on the TiO₂ surface with a contribution of H₂O molecules and/or OH groups [10–12]. However, the nature and strength of O₂^{•−} interactions with the surrounding molecules was not characterized.

In our previous work, paramagnetic O₂^{•−} intermediates formed during the decomposition of H₂O₂ on the TiO₂ surface have been studied employing X- and Q-band CW and pulsed EPR spectroscopy. Exploiting high-resolution pulsed EPR techniques, i.e., 1D and 2D ESEEM (Electron Spin Echo Envelope Modulation) and ENDOR (Electron-Nuclear Double Resonance), weak interactions between the superoxide unpaired electron and the

surrounding protons were quantitatively characterized. This enabled us to modify the model of the $\text{O}_2^{\bullet-}$ with its surrounding environment on the TiO_2 surface [13]. In this work, we found that the superoxide radical with different EPR spectroscopic characteristics is formed in reaction with $\text{Ti}(\text{OR})_4$ ($\text{R} = \text{iPr}, \text{nBu}$) and H_2O_2 in the presence of a KOH solution. The application of pulsed EPR techniques has led to our finding that the stabilization of this $\text{O}_2^{\bullet-}$ is due to proximity to K^+ ion and its involvement in a strong hydrogen-bonding interaction with the surface.

2. Materials and Methods

2.1. Preparation of the Catalysts

The $\text{TiO}_2/\text{O}_2^{\bullet-}$ catalyst studied in our previous work [13] was prepared from $\text{Ti}(\text{OiPr})_4$ exposed to H_2O_2 following the method described in [10]. The dried powder obtained at the end of this procedure was transferred in quartz X- and Q-band EPR tubes, degassed, sealed, and used in the EPR experiments described in [13] (further called “sample I” in this article). It is known that radiolytically or photochemically generated superoxide reacts with tyrosine, forming phenoxyl radicals of tyrosine [14,15]. We aimed to test the appearance of this species in a similar reaction using tyrosine with superoxide on the surface without prior irradiation. The solubility of tyrosine in alcohol is highly pH-dependent [16]. Initially, we tried to initiate a reaction of tyrosine with superoxide by adding tyrosine to the TiO_2 dispersion powder from an alcohol solution or from its mixture with low concentration KOH. EPR spectra of these samples show a rhombic signal consistent with the spectrum of the $\text{O}_2^{\bullet-}$ radical found in sample I. On the contrary, a signal with an axial g-tensor and increased g_{zz} was observed in samples with a higher KOH concentration ($\text{pH} > 10$). Similar results were obtained upon joint addition of peroxide and tyrosine in an alkaline alcohol solution to $\text{Ti}(\text{OCH}(\text{CH}_3)_2)_4$. The presence of an axial EPR signal was also confirmed in the control experiment by adding KOH in methanol without tyrosine to the $\text{TiO}_2/\text{O}_2^{\bullet-}$ catalyst (sample II).

Earlier, in aqueous solutions and mixtures containing alkali metals (M), radicals with similar EPR characteristics attributed to $\text{O}_2^{\bullet-}$ were found, which suggests a special role of M^+ ions in these samples for the radical stabilization. However, no structural EPR support was provided for this hypothesis. Therefore, this paper describes the pulsed EPR characterization of the superoxide radical and its environment in the type II samples containing K^+ ions.

2.2. EPR Measurements

The CW EPR, two-dimensional, four-pulse hyperfine sublevel correlation (HYSCORE, $\pi/2 - \tau - \pi/2 - t_1 - \pi - t_2 - \pi/2 - \tau - \text{echo}$) [17], and Davies pulsed ENDOR ($\pi - t - \pi/2 - \tau - \pi - \tau - \text{echo}$) [18] experiments were performed as previously described elsewhere [13]. The Bruker WIN-EPR software was used for spectral processing.

3. Results and Discussions

3.1. EPR Spectra of Dried $\text{TiO}_2 + \text{H}_2\text{O}_2$

X- and Q-band EPR spectra of a dried sample of TiO_2 (solution of $\text{Ti}(\text{OiPr})_4$ treated with H_2O_2 , sample I) were reported in [13]. They show a signal with rhombic g-tensor produced by the decomposition of H_2O_2 on the TiO_2 surface (Figure S1). The g-tensor principal components (2.024, 2.009, and 2.003) determined from the Q-band spectrum supports the formation of a stable superoxide radical $\text{O}_2^{\bullet-}$ [10], because they are in line with values usually reported for the superoxide on various TiO_2 surfaces ($\text{O}_2^{\bullet-} - \text{Ti}^{4+}$) (see Table S1).

3.2. EPR Spectra in the Presence of KOH

Figures 1 and S2 show Q- and X-band EPR spectra of the radical formed in sample II. The spectra were obtained as a field-swept two-pulse Electron Spin Echo (ESE) signal and its calculated derivative. In contrast to sample I, the shapes of these spectra possess a

typical axial g-tensor anisotropy with principal values $g_{||}(g_{zz}) = 2.10$, $g_{\perp}(g_{x,y}) = 2.002$, and a total width of ~ 20 mT in the X-band. We used the field-sweep ESE because a broad $g_{||}(g_{zz})$ feature was not clearly resolved in CW EPR spectra. The EPR signals with similar g-tensor components $g_{||}(g_{zz}) = 2.10 \pm 0.01$ and $g_{\perp} = 2.005 \pm 0.003$ assigned to the superoxide radical have previously been observed in water solutions with the presence of K_2O , alkaline DMSO solutions, and water/DMSO mixtures (Table 1). One can note that the common factor in all these systems is the presence of alkaline ions. Earlier studies have found a good correlation of the superoxide g_{zz} value with the oxidation state of the nearest metal cation [5,19]. Particularly, a comparison of our data with the reported empirical dependence [5] indicates that $g_{zz} = 2.0227$ for the superoxide in sample I is consistent with its suggested location near Ti^{4+} . In contrast, $g_{zz} = 2.10$ is within the region reported for M^+ and may display the radical location near an alkaline cation in sample II as well as in the compounds shown in Table 1.

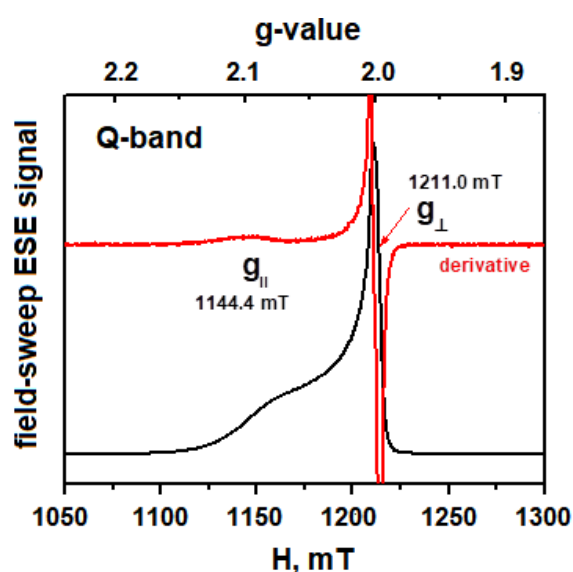


Figure 1. Q-band two-pulse ESE field-sweep spectrum and its first derivative of the radical formed in sample II. Field-sweep ESE generates a spectrum similar in shape to the absorption spectrum produced on the integration of the normal continuous-wave EPR derivative. Microwave frequency is 33.9523 GHz, length of $\pi/2$ pulse is 100 ns, time τ between first and second pulses is 400 ns, and temperature is 15 K.

Table 1. Systems where the EPR signal with axial g-tensor was assigned to a superoxide.

Matrix	$g_{ }(g_{zz})$	$g_{\perp}(g_{x,y})$	Reference
H ₂ O ice (K ₂ O)	2.110		[20]
D ₂ O ice (0.1 mM K ₂ O)	2.110	2.002	[21]
KO ₂ in DMSO/H ₂ O in the presence of ubiquinone-10	2.108	2.004	[22]
Alkaline DMSO	2.098	2.005	[23,24]
10 μ L of 0.5M NaOH/mL of DMSO	2.089	2.007	[25]
TiO ₂ + H ₂ O ₂ + KOH	2.10	2.002	This work

3.3. Pulsed EPR Characterization of the Radical

Interactions between the $O_2^{\bullet-}$ species and its environment in samples I and II were probed using HYSCORE and pulsed ENDOR techniques. Our previous HYSCORE studies of the superoxide in sample I have found only weakly coupled protons, with the anisotropic couplings T not exceeding ~ 2 MHz (Supplementary Materials, Section S1) [13]. These

protons produce cross-features located along an antidiagonal crossing the diagonal of the (++) quadrant at the (ν_{1H}, ν_{1H}) point, where ν_{1H} is the proton Zeeman frequency in the applied magnetic field (Figure S3).

In contrast, the X-band HYSCORE spectrum of sample II (Figure 2) is dominated by a pair of cross-ridges 1_H that significantly deviated from the (ν_{1H}, ν_{1H}) antidiagonal. This indicates the presence of proton(s) with a substantially stronger anisotropic hyperfine interaction [22] than the protons contributing to the spectra of sample I (Figure S3). One can also note that the 1H spectrum in Figure 2 clearly shows additional features $1'_H$ that also deviated from the 1H antidiagonal but oriented in the opposite matter relative to this line. In the course of the analysis described below, we provide evidence that the 1_H and $1'_H$ lines are parts of the same cross-feature located on opposite sides of the diagonal of the (++) quadrant. Lines from weaker coupled protons, elongated along the antidiagonal (ν_{1H}, ν_{1H}) , are also present in the spectra of sample II but possess a lower intensity.

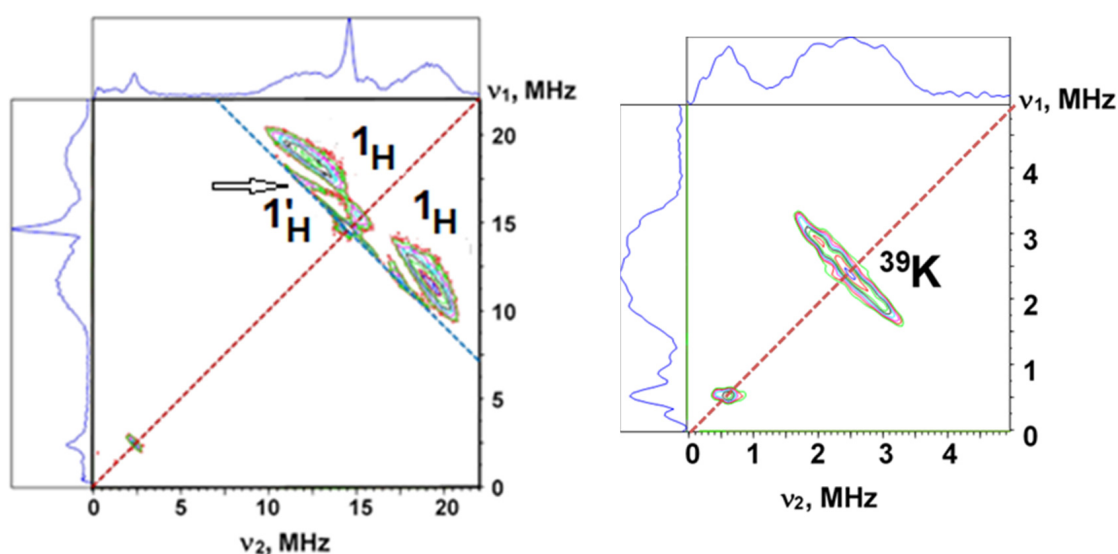


Figure 2. Contour representation of the X- (left) and Q-band (right) HYSCORE spectra of the superoxide radical in sample II. The time τ , between the first and the second microwave pulses, was 136 ns (X) and 200 ns (Q). The spectra were obtained by FT of the 2D time domain patterns containing 256×256 points with a 16 ns step in t_1 and t_2 , which are the intervals between the second and the third microwave pulses, and the third and the fourth microwave pulses, respectively. The microwave frequency was 9.671 GHz (X) and 33.9915 GHz (Q), and the magnetic field was set to 343 mT (X) and 12,125 T (Q), and the temperature was 15 K.

The Q-band HYSCORE spectrum of sample II (Figure 2, right) shows an extended straight ridge around a diagonal frequency of 2.4 MHz with a total length of ~ 2 MHz. This line is produced by the interaction with ^{39}K (nuclear spin $I = 3/2$) possessing a Zeeman frequency of 2.409 MHz in the applied magnetic field 1212.5 mT. The natural abundance of ^{39}K is 93.26%. The second stable isotope ^{41}K has the same nuclear spin and natural abundance of 6.73%. The Zeeman frequency of ^{41}K in the specified field is 1.32 MHz. However, the spectrum in Figure 2 does not contain any features near this frequency on the diagonal line.

4. Discussions

4.1. Analysis of the 1H HYSCORE Spectra

Quantitative analysis of 1H cross-ridges from the HYSCORE spectra of the $O_2^{\bullet-}$ in samples I and II, based on linear regression of contour line shapes in ν_1^2 vs. ν_2^2 coordinates [26], gives isotropic and anisotropic components of hyperfine tensors in axial approximation for protons interacting with the electron spin of the superoxide. Detailed

explanations and results of the analysis are provided in the Supplementary Materials, Section S1.

In particular, a representation of the cross-ridges 1_H from the spectra of sample I prepared with H_2O_2 and D_2O_2 in coordinates ν_1^2 vs. ν_2^2 gives anisotropic hyperfine coupling $T = 2.0 \pm 0.2$ MHz for the contributing proton(s) (Figure S4 and Table S2) [13]. The estimated value of $T \sim 2$ MHz is supported by the negligible deviation of the cross-ridges from the antidiagonal in the experimental spectra. A similar analysis of the cross-ridges 1_H and $1'_H$ with the visible deviation from the antidiagonal (Figure S5) in sample II provides the value of anisotropic coupling of $T \sim 7.0$ MHz, which significantly exceeds the hyperfine coupling of $T \sim 2$ MHz for protons interacting with $O_2^{\bullet-}$ in sample I.

4.2. Evaluation of the Proton Anisotropic Hyperfine Couplings

The anisotropic couplings of $T \sim 2$ MHz and ~ 7 MHz for the superoxide-proton interactions in samples I and II indicate different relative locations of the O–O molecule and protons. The value of ~ 7 MHz is closer to previously reported 1H hyperfine couplings of $T \sim 10$ MHz and 9.8 MHz for a species with similar g-tensor generated on from KO_2 reacting with water in a $H_2O/DMSO$ mixture in the presence of ubiquinone-10 [22] and a Na pre-covered MgO surface [27], respectively. The anisotropic hyperfine tensor for the proton located near the $O_2^{\bullet-}$ is the result of a magnetic dipole–dipole interaction with an unpaired π spin density distributed approximately equally over two oxygens. The tensor depends on a proton position relative to the O–O bond and is generally rhombic [28]. When the interaction between the electron and the proton spins is described by the point dipole approximation the anisotropic parameter is defined by the expression $T = \frac{79}{r^3}$ (MHz) [13], where r is the distance between spins.

The dipole–dipole interaction is described by an axially symmetric tensor with diagonal principal values

$$T = [T_{xx}, T_{yy}, T_{zz}] = T [-1, -1, 2] \quad (1)$$

in the principal axes coordinate, with the z axis directed along the \vec{r} direction.

A proton near the superoxide oxygens O_1 and O_2 , carrying unpaired spin densities ρ_1 and ρ_2 , experiences a local magnetic field, which is a vector sum of two contributions depending on the O_1 –H (r_1) and the O_2 –H (r_2) distances (Figure S9). The principal values of the rhombic hyperfine tensor in this case are [28]

$$T = [1/2 (T_1 + T_2 - 3\delta), -(T_1 + T_2), \frac{1}{2}(T_1 + T_2 + 3\delta)] \quad (2)$$

where $\delta = [T_1^2 + T_2^2 + 2T_1T_2\cos(2\alpha + 2\beta)]^{1/2}$, $T_1 = 79\rho_1/r_1^3$, $T_2 = 79\rho_2/r_2^3$. Equation (2) transforms to the traditional axial form

$$T = [-(T_1 + T_2), -(T_1 + T_2), 2(T_1 + T_2)] \quad (3)$$

for the proton located on the O_1 — O_2 line with $\beta = 180^\circ$ and $\delta = T_1 + T_2$.

The relations between the sides and angles of the triangle HO_1O_2 (Figure S8)

$$r_2^2 = [r_1^2 + r_{O-O}^2 - 2r_1r_{O-O}\cos\beta]^{1/2} \text{ and } \alpha = \arcsin\left[\frac{r_1}{r_2}\sin\beta\right] \quad (4)$$

allow us to define the tensor components based on one distance (r_1 , O_1 –H distance) and one angle (β , angle between H– O_1 and O_1 – O_2).

It has been shown that the unpaired spin density is almost equally ($\rho_{1,2} \sim 0.5$) distributed on the $2p\pi^x$ of each oxygen in superoxide radicals studied in a solution [29], on a MgO surface [30], and generated in TiAlPO-5 [31]. The reported O–O distance in the superoxide varies between 1.32–1.35 Å [29,32–34] and increases under the influence of hydrogen bonds [29,32].

For a direct comparison with the HYSCORE determined values of $T = 2$ [13], 7 (this work) and 10 MHz [22,27], we calculated the term $T_1 + T_2$ from Equation (2), which lacks the rhombic term 3δ and is equal to $T = 39.5 \left[\frac{1}{r_1^3} + \frac{1}{r_2^3} \right]$ for $\rho_1 \approx \rho_2 \approx 0.5$. This term is shown in the form of contours, where each point defines r_1 and β with the selected T (2, 7, or 10 MHz) (Figure 3), i.e., as a function of the O_1 -H distance and the angle β between the H- O_1 and O_1 - O_2 directions. Calculated graphs show that $T = 2$ MHz corresponds to the H- O_1 distance 2.97–3.4 Å for the angles $\beta < 180^\circ$. On the contrary, this distance is ~1.0–1.2 Å less for $T = 7$ or 10 MHz (Table 2).

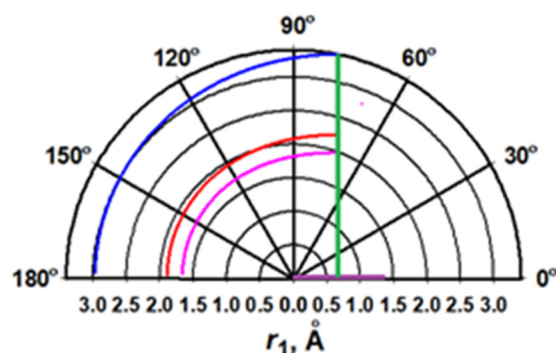


Figure 3. Polar graphs (r_1, β) with representative contours $T = 39.5 \left[\frac{1}{r_1^3} + \frac{1}{r_2^3} \right]$ equal to 2.0 (blue), 7.0 (red), and 10 (pink) MHz calculated for a model with one superoxide oxygen located at the (0,0) point of the coordinates and a second oxygen at the point (1.33 Å, 0°). O_1 - O_2 distance equals to 1.33 Å marked in purple along the line with $\beta = 0^\circ$. Green line normal to r_1 axis corresponds to the middle of the O_1 - O_2 distance. Adapted by permission from Copyright Clearance Center: Springer Nature, Samoilova et al. [13]. Copyright 2022.

Table 2. Distances of a proton location relative to a superoxide radical at different values of the anisotropic hyperfine coupling.

T , MHz	r_1 (H- O_1), Å	β , Degree	r_1 at $\beta = 180^\circ$, Å	r_1 at $\beta = 120^\circ$, Å	References ^a
2	2.97–3.4	180–75	2.97	3.08	[13]
7	1.89–2.24	180–73	1.89	1.95	This work
10	1.67–1.99	180–70	1.67	1.71	[22,27]

^a References, where parameters T from first column were experimentally determined. Adapted by permission from Copyright Clearance Center: Springer Nature, Samoilova et al. [13]. Copyright 2022.

Available models of a hydration shell for the aqueous $O_2^{\bullet-}$ include four water molecules, with two waters forming hydrogen bonds with each oxygen atom (Figure S9). The hydrogen bond lengths vary between 1.72–1.94 Å [30,35,36]. The lower limit of the H- O_1 distance 1.89 Å obtained for $T = 7$ MHz is still within the interval shown above.

4.3. Interaction with ^{39}K Nucleus

^{39}K possesses the nuclear spin $I = 3/2$ with a natural abundance of 93.26%. The orientation disordered HYSCORE spectra of the $S = 1/2$ and $I = 3/2$ system are influenced by hyperfine and nuclear quadrupole interactions. Both of them are anisotropic. Available data about the nuclear quadrupole coupling constant in $^{39}\text{K}^+$ state indicate that it is quite small [37,38]. Model simulations of the HYSCORE spectra from $I = 3/2$ nuclei with hyperfine and nuclear quadrupole tensors satisfying the conditions [$\nu_1 > A_{ZZ} > Q_{ZZ}$] have shown that the hyperfine interaction creates cross-ridges normal to the diagonal line in the (++) quadrant, whereas the nuclear quadrupole interaction produces an additional splitting of these cross-features in the direction parallel to the diagonal [39]. This simple manual is helpful for the qualitative analysis of the observed spectrum from ^{39}K (Figure 2).

The spectrum consists of a straight segment normal to the diagonal of the (++) quadrant and is located symmetrically relative to the ($\nu_{39\text{K}}, \nu_{39\text{K}}$) diagonal point. The length of the ridge is about ~ 2 MHz along each coordinate. A projection of the spectrum on each coordinate and stacked presentation of the spectrum shows a weakly resolved triplet structure of the ridge with the hyperfine splitting $\Delta \sim 1$ MHz between cross-peaks with permuted coordinates of ~ 2 and 3 MHz. The spectrum does not show any additional splitting of the ridge along the diagonal, assuming the small value of the quadrupole coupling constant of ^{39}K [39].

The crystal structure of an α -potassium superoxide shows an octahedral environment of the superoxide ion near K^+ ions with smallest contact distances of 2.71 Å in the direction parallel to the O–O bond and another 2.92 Å away, in the direction approximately normal to the O–O bond [40]. The calculated value of the principal component ($T_1 + T_2$) of the hyperfine tensor defined by Equation (2) for the two indicated locations of $^{39}\text{K}^+$ using formulae $T = (3.7/2)[1/r_1^3 + 1/r_2^3]$ is equal to 0.12 and 0.148 MHz, respectively. The anisotropic width of the single-quantum transitions in the powder spectrum $3T/2$ does not explain the line splitting ~ 1 MHz from ^{39}K , as detected in the HYSORE spectrum. Consequently, there remains only one source resulting in the observed line shape—the isotropic hyperfine interaction. However, the simulation of spectra with parameters $a \sim 1$ MHz and $T \sim 0.15$ MHz did not reproduce the presence of a spectral intensity around the diagonal between two peaks with a ~ 1 MHz splitting. Additional ideas about hyperfine interactions between ^{39}K and the $\text{O}_2^{\bullet-}$ can be obtained by taking into account the available data on hyperfine couplings between a superoxide and ^{23}Na or ^{133}Cs on the MgO surface.

4.4. Comparison with Superoxide on a Na or Cs Pre-Covered MgO Surface

The EPR spectrum of superoxide species formed on a Na pre-covered MgO surface [27] shows a formation of two species with g_{zz} values equal to 2.091 and 2.14. The $g_{x,y}$ components of both species are close to $g = 2$ and produce a single intensive line with a width of 1.5–2.0 mT in the spectrum. The species with $g_{zz} = 2.091$ have been assigned to superoxide ions on Mg^{2+} matrix sites. The value $g_{zz} = 2.14$ is within the range typical for superoxide anions stabilized on monovalent cations; thus, the corresponding EPR signal was designated as a surface $\text{O}_2^{\bullet-} - \text{Na}^+$ adduct.

The HYSORE spectra collected in the $g_{x,y}$ area of the Na/MgO sample contain cross-features from the ^{23}Na and ^1H nuclei (Figure S10). Two of them belong to ^{23}Na with strong and weak hyperfine couplings ~ 17 MHz and $\sim <3$ MHz, respectively. The ^1H spectrum consists of two extended ridges with a clearly visible deviation from the antidiagonal crossing ($\nu_{1\text{H}}, \nu_{1\text{H}}$) point of the diagonal, indicating a strong anisotropic interaction between the superoxide and a proton. Computer simulations of the spectrum have provided hyperfine tensors $a = -15 \pm 2$ MHz, $T = (-0.1, 3.1, -3.0)$ MHz (± 0.5 MHz) for the strongly coupled ^{23}Na from the $\text{O}_2^{\bullet-} - \text{Na}^+$ adduct and $a = -5.0 \pm 0.5$ MHz, $T = (-9.8, 19.6, -9.8)$ MHz (± 0.1 MHz) for the proton that produced extended cross-ridges. It was suggested that this proton belongs to the superoxide stabilized on the Mg^{2+} matrix site in the proximity of a surface OH^- . Our analysis (Figure 3) shows that the ^1H coupling of $T \sim 10$ MHz indicates the formation of an H-bond between the superoxide and proton with an O–H distance of ~ 1.7 – 2.0 Å. Furthermore, the authors have proposed that the line around the diagonal ($\nu_{\text{Na}}, \nu_{\text{Na}}$) point is produced by remote ^{23}Na nuclei that are randomly distributed between 3.5 Å and 4.5 Å away (i.e., $0.5 > |T| > 0.2$ MHz in the point dipole approximation), and the species of both g_{zz} contribute to this feature [27].

To compare the experimental and calculated spectra, this feature was calculated using a single hyperfine tensor $a = -2.5$ MHz, $T = (-0.5, -0.5, 1.0)$ MHz (Figure S10). On the other hand, we estimated $T_{\text{max}} = (20.9/2)[1/r_1^3 + 1/r_2^3]$ for two models of the ^{23}Na location relative to the superoxide (O–O length 1.33 Å) using a Na–O distance of 2.38–2.39 Å reported for the orthorhombic structure of sodium superoxide [41,42]. The corresponding values are $T_{\text{max}} \sim 1$ MHz and 1.5 MHz for the ^{23}Na locations on the line extending the O–O bond and normal to the middle of the O–O bond that is consistent with the value of

$T_{\max}/2$ used for calculating the spectrum. This estimate shows that the signal assigned to randomly distributed ^{23}Na nuclei at distances in the range between 3.5 Å and 4.5 Å can be produced just by one nucleus located at the Na–O distance found in the crystal structures. More convincing conclusions about the nature of the signal from weakly coupled Na could be supported by the relative intensities of two sodium signals which are not available from the published spectra.

The increased hyperfine parameters for strongly coupled ^{23}Na is explained by the formation of the ionic sodium superoxide Na^+O_2^- as symmetrical triangular molecules with an interatomic distance of 1.96 Å that was deduced from vibrational spectra [43]. One can recalculate the characteristic hyperfine parameters of the $^{23}\text{Na}^+\text{O}_2^{\bullet-}$ species obtained in this work for a superoxide interacting with a nucleus of $^{39}\text{K}^+$. The ratio of $^{23}\text{Na}/^{39}\text{K}$ magnetic moments is 5.56. Then, the parameters $|a| = 15$ MHz and $|T| = 3$ MHz found for the $^{23}\text{NaO}_2$ species will give formal values of $a = 2.7$ MHz and $T = 0.54$ MHz for ^{39}K . The ratio of the atomic isotropic hyperfine constants 927.1 MHz (^{23}Na , 3s) and 228.5 MHz (^{39}K , 4s) [44] calculated for unit spin density is 4.06. It leads to a decreasing a value of 0.67 MHz. Another possible factor that may reduce the hyperfine parameters of ^{39}K compared to ^{23}Na is the larger value of its ionic radius (1.02 Å for ^{23}Na and 1.38 Å for ^{39}K). Simulations of the ^{39}K HYSCORE spectra with estimated parameters $a = 0.6$ – 0.7 MHz and $T = 0.6$ MHz confirm the increased total length of the cross-ridge and its line shape without well pronounced maxima (Figure S11). Thus, the recalculation analysis assuming similar structural motifs of the MO_2 species predicts significantly lower hyperfine couplings for ^{39}K . However, the value of the anisotropy parameter is greater than the calculated ~ 0.15 MHz using the crystallographic structure. That increase provides an extended line shape from ^{39}K , which is consistent with the experimental HYSCORE spectra.

DFT calculations of the hyperfine parameters for $\text{O}_2^{\bullet-}$ in Na/MgO were performed for different elements of the MgO surface [27]. Based on the analysis of the full set of \mathbf{g} and \mathbf{A} tensors, the NaO_2 species formed on an edge site of the MgO surface, where O_2 is simultaneously bound to Na and to MgO, give the best description of the large g_{zz} and the ^{23}Na hyperfine interaction observed in the EPR experiments. On the other hand, the DFT analysis of the ^1H tensor determined from the HYSCORE spectrum of $\text{O}_2^{\bullet-}$ in Na/MgO has not been carried out even for the proposed $\text{O}_2^{\bullet-}/\text{HMgO}$ center, although this tensor possesses an $a_{\text{iso}} = -5$ MHz and $T_{\max} = 19.6$ MHz, which significantly exceeds the $a_{\text{iso}} \sim 0$ MHz and $T_{\max} \sim 10$ MHz reported for $\text{O}_2^{\bullet-}$ at the surface of MgO [45].

One can note that the exchangeable proton with $T_{\max} \sim 20$ MHz was found in the HYSCORE spectra of the superoxide in the $\text{KO}_2/\text{DMSO}/\text{H}_2\text{O}$ mixture in the presence of ubiquinone-10 [24]. However, the X-band HYSCORE spectra obtained in this work were not suitable for the detection of ^{39}K signals due to a low Zeeman frequency in this band.

Other experimental examples relevant to this work are EPR studies of $^{23}\text{NaO}_2$, $^{39}\text{KO}_2$, $^{87}\text{RbO}_2$, and $^{133}\text{CsO}_2$ in rare gas matrices [46] and superoxides on a $^{133}\text{Cs}/\text{MgO}$ surface [47]. Similar to Table 1, the g_{zz} component of these species varies between 2.10–2.12, and the alkali metals ^{23}Na and ^{133}Cs produce a resolved hyperfine splitting of the g_{zz} and $g_{xx,yy}$ components presented in Table 3.

Table 3. EPR parameters of MO_2 species in a rare gas and on a MgO surface.

Sample	g_{zz}	T_{11}	T_{22}	T_{33}	a_{iso}	A_0	$\rho \times 10^{-3}$	Ref. ^a
$^{23}\text{NaO}_2$	2.111	−2.8	1.68	−1.12	9	927.1	9.7	[46]
$\text{O}_2^{\bullet-}$ on Na/MgO	2.14	−0.1	3.1	−3.0	−15	927.1	16.2	[27]
$^{133}\text{CsO}_2$	2.107	−0.56	0.84	−0.28	14	2464	5.7	[46]
$\text{O}_2^{\bullet-}$ on Cs/MgO	2.120	5.1	2.6	−7.7	29.6	2464	12.0	[47]

^a T_{ii} components of an anisotropic tensor, isotropic constant a_{iso} , and atomic isotropic hyperfine constant A_0 are in MHz.

A comparison with rare-gas matrix-trapped MO_2 molecules shows that the surface-stabilized complexes are characterized by larger a_{iso} and g_{zz} parameters. The differences between isolated MO_2 molecules and surface-adsorbed NaO_2/MgO species have been examined with the help of DFT calculations, which illustrated the role of the matrix in the stabilization of the superoxide with particular magnetic characteristics [27]. A set of surface sites was compatible with the observed experimental results, which are characterized by a mutual interaction between the superoxide anion and the Mg^{2+} matrix ions and adsorbed Na^+ species. Particularly, in the case of the surface-stabilized NaO_2 complex, the unpaired electron is localized in a π^* orbital lying in the $\text{O}_2\text{--Na}$ plane, whereas the π^* orbital hosting the unpaired electron is found to be perpendicular to the $\text{M}(\text{OO})$ plane for matrix-trapped NaO_2 in the rare gas. This difference will influence the hyperfine interaction with the alkaline atom nucleus [46].

5. Conclusions

Our experiments with the $\text{TO}_2 \dots \text{O}_2^{\bullet-}$ catalyst obtained with the joint addition of peroxide and a KOH solution of alcohol show the formation of the superoxide radical with the atypical $g_{\text{zz}} = 2.10$. A similar EPR signal was previously observed in various systems containing alkaline ions that allowed us to suggest the special role of K^+ ions in the $\text{O}_2^{\bullet-}$ stabilization. However, ^{39}K nucleus(i) did not produce any resolved features in the reported EPR spectra. In this work, we applied 2D HYSCORE spectroscopy to characterize hyperfine interactions between the $\text{O}_2^{\bullet-}$ and the ^{39}K and ^1H nuclei in its environment. Q-band HYSCORE spectra have shown the presence of ^{39}K near the superoxide. A comparison of the magnetic characteristics and electronic configuration defining the isotropic coupling of ^{39}K with ^{23}Na in Na/MgO [27] allowed us to predict significantly smaller ^{39}K hyperfine couplings for the similar structural MO_2 motifs. The estimated values give a reasonable agreement between the calculated and experimental ^{39}K HYSCORE spectra. Another finding of this superoxide is the existence of a strongly coupled ^1H with the anisotropic coupling $T \sim 7$ MHz, which suggests the formation of an H-bond with an O–H distance of $<2\text{\AA}$. So far, an interaction with the closely located alkaline ion and the strongly coupled proton $T \sim 10$ MHz has been reported for the $\text{O}_2^{\bullet-}$ on Na/MgO only [27]. However, two different $\text{O}_2^{\bullet-}$ species with $g_{\text{zz}} = 2.014$ and 2.091 were present in this sample, and strongly coupled ^{23}Na with $a = 15$ MHz and the ^1H with anisotropic coupling $T = 9.8$ MHz were assigned to different species, $-\text{O}_2^{\bullet-}/\text{NaMgO}$ and $\text{O}_2^{\bullet-}/\text{HMgO}$, respectively. Only one type of $\text{O}_2^{\bullet-}/\text{KTiO}_2$ species with $g_{\text{zz}} = 2.10$ was found in our work. This means that signals from ^{39}K and a strongly coupled proton with $T \sim 7$ MHz in the HYSCORE spectra are produced by interactions with this superoxide and should be considered as the elements of its structure. Therefore, independent data to support the hypothesis that the presence of a stable superoxide radical in systems containing alkali metals requires the simultaneous proximity of M^+ ion(s) and the formation of a hydrogen bond with its environment are still needed.

Supplementary Materials: The following supporting information can be downloaded at: <https://www.mdpi.com/article/10.3390/inorganics11070274/s1>, Figure S1: X- and Q-band EPR spectra of the superoxide radical in sample I; Figure S2: X-band two-pulse ESE field-swept spectrum and its first derivative of the TiO_2 surface produced from $\text{Ti}(\text{OiPr})_4$ exposed to $\text{H}_2\text{O}_2/\text{KOH}$; Figure S3: Contour representation of the HYSCORE spectra of the superoxide radical in the sample I (a) and in the similar sample prepared using D_2O_2 (b); Figure S4: Plots of cross-ridges 1_{H} from HYSCORE spectra of the superoxide radical in sample I in the $(\nu_1)^2$ vs. $(\nu_2)^2$ coordinate system; Figure S5: Plots of cross-ridges 1_{H} and $1_{\text{H}'}$ from HYSCORE spectrum of the superoxide radical in sample II in the $(\nu_1)^2$ vs. $(\nu_2)^2$ coordinate system; Figure S6: Q-band field-sweep 2-pulse ESE spectrum (a) and Q-band Davies ENDOR spectra (b) of the superoxide radical in sample I; Figure S7: Q-band Davies ENDOR spectrum of the superoxide radical in sample II; Figure S8: Definition of the distances and angles describing the location of the proton relative to O_1 and O_2 of the superoxide radical; Figure S9: Structural model of $[\text{O}_2(\text{H}_2\text{O})_4]^-$; Figure S10: Experimental and simulated HYSCORE spectra of the $\text{O}_2^{\bullet-}$ species on Na/MgO ; Figure S11: Experimental and simulated ^{39}K HYSCORE spectra; Table S1: g-tensors

assigned to the $O_2^{\bullet-}$ radical in different TiO_2 samples; Table S2: 1H hyperfine tensor parameters determined from linear regressions of the cross-ridges; Section S1: Square frequency fitting of the 1H HYSCORE spectra and its comparison with the pulsed ENDOR data [4,10,13,22,26,27,29,31,35,36,48–56].

Author Contributions: Conceptualization, R.I.S. and S.A.D.; methodology, R.I.S. and S.A.D.; validation, R.I.S. and S.A.D.; resources, S.A.D.; writing—original draft preparation, S.A.D.; writing—review and editing, S.A.D. and R.I.S.; project administration, S.A.D.; funding acquisition, S.A.D. All authors have read and agreed to the published version of the manuscript.

Funding: This work was supported by Grant DE-FG02-08ER15960 (S.A.D.) from the Chemical Sciences, Geosciences and Biosciences Division, the Office of Basic Energy Sciences, and the Office of Sciences, U.S. Department of Energy.

Institutional Review Board Statement: Not applicable.

Informed Consent Statement: Not applicable.

Data Availability Statement: All data and information recorded or analyzed throughout this study are included in this paper.

Acknowledgments: The authors are grateful to Andrei Astashkin (University of Arizona) for very useful discussions and Quan Lam for a critical reading of the manuscript.

Conflicts of Interest: The authors declare no conflict of interest.

References

1. Hayyan, M.; Hashim, M.A.; AlNashef, I.M. Superoxide Ion: Generation and Chemical Implications. *Chem. Rev.* **2016**, *116*, 3029–3085. [CrossRef]
2. Afanas'ev, I.B. The Oxygen Radical-anion O_2^- in Chemical and Biochemical Processes. *Russ. Chem. Rev.* **1979**, *48*, 527–549. [CrossRef]
3. Sawyer, D.T.; Valentine, J.S. How Super Is Superoxide? *Acc. Chem. Res.* **1981**, *14*, 393–400. [CrossRef]
4. Anpo, M.; Che, M.; Fubini, B.; Garrone, E.; Giamello, E.; Paganini, M.C. Generation of Superoxide Ions at Oxide Surfaces. *Top. Catal.* **1999**, *8*, 189–198. [CrossRef]
5. Che, M.; Tench, A.J. Characterization and Reactivity of Molecular Oxygen Species on Oxide Surfaces. *Adv. Catal.* **1983**, *32*, 1–148.
6. Kokorin, A.I. Electron Spin Resonance of Nanostructured oxide semiconductors. In *Chemical Physics of Nanostructured Semiconductors*; Kokorin, A.I., Bahnmann, D.W., Eds.; CRC Press: Boca Raton, FL, USA, 2003; Chapter 8, pp. 203–263.
7. Chiesa, M.; Giamello, E.; Che, M. EPR Characterization and Reactivity of Surface-Localized Inorganic Radicals and Radical Ions. *Chem. Rev.* **2010**, *110*, 1320–1347. [CrossRef]
8. Sobańska, K.; Krasowska, A.; Mazur, T.; Podolska-Serafin, K.; Pietrzyk, P.; Sojka, Z. Diagnostic Features of EPR Spectra of Superoxide Intermediates on Catalytic Surfaces and Molecular Interpretation of Their g and A Tensors. *Top. Catal.* **2015**, *58*, 796–810. [CrossRef]
9. Giamello, E.; Rumori, P.; Geobaldo, F.; Fubini, B.; Paganini, M.C. The Interaction between Hydrogen Peroxide and Metal Oxides: EPR Investigations. *Appl. Magn. Res.* **1996**, *10*, 173–192. [CrossRef]
10. Dewkar, G.K.; Nikalje, M.D.; Sayyed, I.A.; Paraskar, A.S.; Jagtap, H.S.; Sudalai, A. An Exceptionally Stable Ti Superoxide Radical Ion: A Novel Heterogeneous Catalyst for the Direct Conversion of Aromatic Primary Amines to Nitro Compounds. *Angew. Chem. Int. Ed.* **2001**, *40*, 405–408. [CrossRef]
11. Dewkar, G.K.; Shaikh, T.M.; Pardhy, S.; Kulkarni, S.S.; Sudalai, A. Titanium superoxide catalyzed selective oxidation of phenols to p-quinones with aq. H_2O_2 . *Indian J. Chem. B* **2005**, *44*, 1530–1532. [CrossRef]
12. Reddy, R.S.; Shaikh, T.M.; Rawat, V.; Karabal, P.U.; Dewkar, G.; Suryavanshi, G.; Sudalai, A. A Novel Synthesis and Characterization of Titanium Superoxide and its Application in Organic Oxidative Processes. *Catal. Surv. Asia* **2010**, *14*, 21–32. [CrossRef]
13. Samoilova, R.I.; Dikanov, S.A. Local environment of superoxide radical formed on the TiO_2 surface produced from $Ti(OiPr)_4$ exposed to H_2O_2 . *Appl. Magn. Reson.* **2022**, *53*, 1089–1104. [CrossRef]
14. Jin, F.; Leitich, J.; von Sonntag, C. The superoxide radical reacts with tyrosine-derived phenoxyl radicals by addition rather than by electron transfer. *J. Chem. Soc. Perkin. Trans. II* **1993**, 1583–1588. [CrossRef]
15. Schunemann, V.; Lendzian, F.; Jung, C.; Contzen, J.; Barra, A.-L.; Sligar, S.G.; Trautwein, A.X. Tyrosine Radical Formation in the Reaction of Wild Type and Mutant Cytochrome P450_{cam} with Peroxy. *J. Biol. Chem.* **2004**, *279*, 10919–10930. [CrossRef] [PubMed]
16. Hitchcock, D.I. The solubility of tyrosine in acid and alkali. *J. Gen. Physiol.* **1924**, *6*, 747–757. [CrossRef] [PubMed]
17. Höfer, P.; Grupp, A.; Nebenführ, H.; Mehring, M. Hyperfine Sublevel Correlation (HYSCORE) spectroscopy: A 2D ESR investigation of the squaric acid radical. *Chem. Phys. Lett.* **1986**, *132*, 279–282. [CrossRef]
18. Davies, E.R. A New Pulse Endor Technique. *Phys. Lett. A* **1974**, *47*, 1–2. [CrossRef]
19. Lunsford, J.H. ESR of Adsorbed Oxygen Species. *Catal. Rev.* **1973**, *8*, 135–157. [CrossRef]

20. Symons, M.C.R.; Eastland, G.W.; Denny, L.R. Effect of Solvation on the Electron Spin Resonance Spectrum of the Superoxide ion. *J. Chem. Soc. Faraday Trans. I* **1980**, *76*, 1868–1874. [[CrossRef](#)]
21. Narayana, P.A.; Suryanarayana, D.; Kevan, L. Electron Spin-Echo Studies of the Solvation Structure of Superoxide ion (O_2^-) in Water. *J. Am. Chem. Soc.* **1982**, *104*, 3552–3555. [[CrossRef](#)]
22. Samoilova, R.I.; Crofts, A.R.; Dikanov, S.A. Reaction of Superoxide Radical with Quinone Molecules. *J. Phys. Chem. A* **2011**, *115*, 11589–11593. [[CrossRef](#)]
23. Haseloff, R.; Ebert, B.; Damerau, W. Superoxide generation in alkaline dimethyl sulfoxide. *Anal. Chim. Acta.* **1989**, *218*, 179–184. [[CrossRef](#)]
24. Krager, K. *Superoxide in Aprotic Solvents*; The University of Iowa: Iowa City, IA, USA, 2003.
25. Hyland, K.; Auclair, C. The Formation of Superoxide Radical Anions by a Reaction Between O_2 , OH^- and Dimethyl Sulfoxide. *Biochem. Biophys. Res. Comm.* **1981**, *102*, 531–537. [[CrossRef](#)] [[PubMed](#)]
26. Dikanov, S.A.; Bowman, M.K. Cross-peak lineshape of two-dimensional ESEEM spectra in disordered $S=1/2$, $I=1/2$ spin system. *J. Magn. Reson., Ser. A* **1995**, *116*, 125–128. [[CrossRef](#)]
27. Napoli, F.; Chiesa, M.; Giamello, E.; Preda, G.; Di Valentin, C.; Pacchioni, G. Formation of Superoxo Species by Interaction of O_2 with Na Atoms Deposited on MgO Powders: A Combined Continuous-Wave EPR (CW-EPR), Hyperfine Sublevel Correlation (HYSCORE) and DFT Study. *Chem. Eur. J.* **2010**, *16*, 6776–6785. [[CrossRef](#)]
28. Randall, D.W.; Gelasco, A.; Caudle, M.T.; Pecoraro, V.L.; Britt, R.D. ESE-ENDOR and ESEEM Characterization of Water and Methanol Ligation to a Dinuclear Mn(III)Mn(IV) Complex. *J. Am. Chem. Soc.* **1997**, *119*, 4481–4491. [[CrossRef](#)]
29. Janik, I.; Tripathi, G.N.R. The nature of the superoxide radical anion in water. *J. Chem. Phys.* **2013**, *139*, 014302. [[CrossRef](#)] [[PubMed](#)]
30. Chiesa, M.; Giamello, E.; Paganini, M.C.; Sojka, Z.; Murphy, D.M. Continuous Wave Electron Paramagnetic Resonance Investigation of the Hyperfine Structure of $^{17}O_2^-$ Adsorbed on the MgO Surface. *J. Chem. Phys.* **2002**, *116*, 4266–4274. [[CrossRef](#)]
31. Maurelli, S.; Vishnuvarthan, M.; Berlier, G.; Chiesa, M. NH_3 and O_2 interaction with tetrahedral Ti^{3+} ions isomorphously substituted in the framework of $TiAlPO_5$. A combined pulse EPR, pulse ENDOR, UV-Vis and FT-IR study. *Phys. Chem. Chem. Phys.* **2012**, *14*, 987–995. [[CrossRef](#)] [[PubMed](#)]
32. Dietzel, P.D.C.; Kremer, R.K.; Jansen, M. Tetraorganylammonium Superoxide Compounds: Close to Unperturbed Superoxide Ions in the Solid State. *J. Am. Chem. Soc.* **2004**, *126*, 4689–4696. [[CrossRef](#)]
33. Seyed, H.; Jansen, M. A novel access to ionic superoxides and the first accurate determination of the bond distance in O_2^- . *J. Chem. Soc. Dalton Trans.* **1998**, *6*, 875–876. [[CrossRef](#)]
34. Halverson, F. Comments on Potassium Superoxide Structure. *J. Phys. Chem. Solids* **1962**, *23*, 207–214. [[CrossRef](#)]
35. Antonchenko, V.Y.; Kryachko, E.S. Interaction of Superoxide O_2^- with Water Hexamer Clusters. *Chem. Phys.* **2006**, *327*, 485–493. [[CrossRef](#)]
36. Antonchenko, V.Y.; Kryachko, E.S. Structural, Energetic, and Spectroscopic Features of Lower Energy Complexes of Superoxide Hydrates $O_2^-(H_2O)_{1-4}$. *J. Phys. Chem. A* **2005**, *109*, 3052–3059. [[CrossRef](#)] [[PubMed](#)]
37. Barkhuijsen, H.; de Beer, R.; Deutz, A.F.; van Ormondt, D.; Völkel, G. Observation of Potassium Hyperfine Interactions in X-irradiated KH_2AsO_4 through the Method of Electron Spin Echo Envelope Modulation. *Solid State Commun.* **1984**, *49*, 679–684. [[CrossRef](#)]
38. Nellutla, S.; Morley, G.W.; van Tol, J.; Pati, M.; Dalal, N.S. Electron Spin Relaxation and ^{39}K Pulsed ENDOR Studies on Cr^{5+} -doped K_3NbO_8 at 9.7 and 240 GHz. *Phys. Rev. B* **2008**, *78*, 054426. [[CrossRef](#)]
39. Gutjahr, M.; Böttcher, R.; Pöpl, A. Analysis of Correlation Patterns in Hyperfine Sublevel Correlation Spectroscopy of $S = 1/2$, $I = 3/2$ Systems. *Appl. Magn. Reson.* **2002**, *22*, 401–414. [[CrossRef](#)]
40. Abrahams, S.C.; Kalnajs, J. The Crystal Structure of α -Potassium Superoxide. *Acta Crystallogr.* **1955**, *8*, 503–506. [[CrossRef](#)]
41. Carter, G.F.; Templeton, D.H. Polymorphism of Sodium Superoxide. *J. Am. Chem. Soc.* **1953**, *75*, 5247–5249. [[CrossRef](#)]
42. Deng, N.; Yang, G.; Wang, W.; Qiu, Y. Structural Transitions and Electronic Properties of Sodium Superoxide at High Pressures. *RSC Adv.* **2016**, *6*, 67910–67915. [[CrossRef](#)]
43. Smardzewski, R.R.; Andrews, L. Raman Spectra of the Products of Na and K Atom Argon Matrix Reactions with O_2 Molecules. *J. Chem. Phys.* **1972**, *57*, 1327–1333. [[CrossRef](#)]
44. Morton, J.R.; Preston, K.F. Atomic Parameters for Paramagnetic Resonance Data. *J. Magn. Reson.* **1978**, *30*, 577–583. [[CrossRef](#)]
45. Giamello, E.; Ugliengo, P.; Garrone, E.; Che, M.; Tench, A.J. Experimental Evidence for the Hyperfine Interaction between a Surface Superoxide Species on MgO and a Neighbouring Hydroxylic Proton. *J. Chem. Soc. Faraday Trans. I* **1989**, *85*, 3987–3994. [[CrossRef](#)]
46. Lindsay, D.M.; Herschbach, D.R.; Kwiram, A.L. ESR of Matrix Isolated Alkali Superoxides. *Chem. Phys. Lett.* **1974**, *25*, 175–181. [[CrossRef](#)]
47. Chiesa, M.; Paganini, M.C.; Giamello, E.; Murphy, D.M. Partial Ionization of Cesium Atoms at Point Defects over Polycrystalline Magnesium Oxide. *J. Phys. Chem. B* **2001**, *105*, 10457–10460. [[CrossRef](#)]
48. Antcliff, K.L.; Murphy, D.M.; Griffiths, E.; Giamello, E. The interaction of H_2O_2 with exchanged titanium oxide systems (TS-1, TiO_2 , [Ti]-APO-5, Ti-ZSM-5). *Phys. Chem. Chem. Phys.* **2003**, *5*, 4306–4316. [[CrossRef](#)]
49. Ramaswamy, V.; Awati, P.; Ramaswamy, A.V. Epoxidation of indene and cyclooctene on nanocrystalline anatase titania catalyst. *Top. Catal.* **2006**, *38*, 251–259. [[CrossRef](#)]

50. Tengvall, P.; Lundström, I.; Sjöqvist, L.; Elwing, H.; Bjursten, L.M. Titanium-hydrogen peroxide interaction: Model studies of the influence of the inflammatory response on titanium implants. *Biomaterials* **1989**, *10*, 166–175. [[CrossRef](#)]
51. Green, J.; Carter, E.; Murphy, D.M. Interaction of molecular oxygen with oxygen vacancies on reduced TiO₂: Site specific blocking by probe molecules. *Chem. Phys. Lett.* **2009**, *477*, 340–344. [[CrossRef](#)]
52. Carter, E.; Carley, A.F.; Murphy, D.M. Evidence for O²⁻ Radical Stabilization at Surface Oxygen Vacancies on Polycrystalline TiO₂. *J. Phys. Chem. C* **2007**, *111*, 10630–10638. [[CrossRef](#)]
53. Liu, F.; Feng, N.; Wang, Q.; Xu, J.; Qi, G.; Wang, W.; Deng, F. Transfer Channel of Photoinduced Holes on a TiO₂ Surface As Revealed by Solid-State Nuclear Magnetic Resonance and Electron Spin Resonance Spectroscopy. *J. Am. Chem. Soc.* **2017**, *139*, 10020–10028. [[CrossRef](#)] [[PubMed](#)]
54. Rahemi, V.; Trashin, S.; Hafideddine, Z.; Meynen, V.; Van Doorslaer, S.; De Wael, K. Enzymatic sensor for phenols based on titanium dioxide generating surface confined ROS after treatment with H₂O₂. *Sens. Actuators B Chem.* **2019**, *283*, 343–348. [[CrossRef](#)]
55. Yu, J.; Chen, J.; Li, C.; Wang, X.; Zhang, B.; Ding, H. ESR Signal of Superoxide Radical Anion Adsorbed on TiO₂ Generated at Room Temperature. *J. Phys. Chem. B* **2004**, *108*, 2781–2783. [[CrossRef](#)]
56. Dikanov, S.A.; Tyryshkin, A.M.; Bowman, M.K. Intensity of cross-peaks in HYSCORE spectra of S = 1/2, I = 1/2 spin systems. *J. Magn. Reson.* **2000**, *144*, 228–242. [[CrossRef](#)] [[PubMed](#)]

Disclaimer/Publisher’s Note: The statements, opinions and data contained in all publications are solely those of the individual author(s) and contributor(s) and not of MDPI and/or the editor(s). MDPI and/or the editor(s) disclaim responsibility for any injury to people or property resulting from any ideas, methods, instructions or products referred to in the content.